Anisotropic scattering in the goniopolar metal NaSn$_2$As$_2$

Yaxian Wang [*] and Prineha Narang [†]

John A. Paulson School of Engineering and Applied Sciences, Harvard University, Cambridge, Massachusetts 02138, USA

Recent experimental discoveries in axis-dependent conduction polarity, or *goniopolarity*, have observed that the charge carriers can conduct like either electrons or holes depending on the crystallographic direction they travel along in layered compounds such as NaSn$_2$As$_2$. The original theoretical proposal is based on the opposite signs of the carrier effective mass, or the curvature of the Fermi surface, without examining the effect of electron lifetimes, thus leaving a crucial question to address. To elucidate this unusual transport behavior, we present an *ab initio* study of electron scattering in such systems. We study different microscopic scattering mechanisms in NaSn$_2$As$_2$, and we present the electron-phonon scattering time distribution on its Fermi surface in momentum space, the open concave shape of which is proposed to be the origin of the axis-dependent conduction polarity. Further, we obtain the overall anisotropic lifetime tensors in real space at different electron chemical potentials and temperatures, and we discuss how they contribute to the macroscopic thermopower. While we find that the contribution of the in-plane and cross-plane lifetimes exhibits a similar trend, the concave portion of the Fermi surface alters the electron motion significantly in the presence of a magnetic field, thus flipping the conduction polarity as measured via the Hall effect. Our calculations and analysis of NaSn$_2$As$_2$, in comparison with similar systems, also suggest the strong possibility of hydrodynamic electron flow in the system. Finally, our work has implications for anisotropic electron lifetimes in a broad class of goniopolar materials and provides key, general insights into electron scattering on open Fermi surfaces.

I. INTRODUCTION

Transport in metals and semimetals is extremely sensitive to the dynamics at (and near) the Fermi level. Therefore, the geometric shape, or topology, of the Fermi surface can determine the conductivity tensor following Mott's relation: $\sigma_{ij}(E_F) = q^2 N(E_F) \tau_{ij}(E_F) m_{ij}^{*-1}(E_F)$, where q is the electron charge, N is the carrier density, and τ_{ij} and m_{ij}^{*-1} are the scattering time and reverse effective-mass tensors evaluated at the Fermi level E_F [1]. The latter can be visualized as the curvature of the energy band or the Fermi surface [2], whose topology can dramatically alter the electron transport, and thus give rise to exotic phenomena [3–10].

Recent findings in axis-dependent conduction polarity, or *goniopolarity*, reveal that charge carriers can be "entangled" with the direction they travel in layered compound NaSn$_2$As$_2$ [11], originating from its hyperboloid open Fermi surface. This means that in NaSn$_2$As$_2$, the band curvature, or the carrier effective mass, has opposite signs along the in-plane x, y (m_{xx}^* or m_{yy}^*) versus the cross-plane z (m_{zz}^*) axes, thus altering the sign of its thermopower, which is related to the electrical conductivity as $\alpha_{ij} = -\frac{\pi^2 k_B^2 T}{3q} \frac{\sigma'_{ij}}{\sigma_{ij}}$, with σ'_{ij} being the energy derivative of σ_{ij}. Meanwhile, delafossites PdCoO$_2$ and PtCoO$_2$ are expected, based on their Seebeck coefficients [12,13], to exhibit similar behavior due to their anisotropic effective-mass tensors on their open, nearly cylindrical Fermi surfaces. While previous theoretical approaches were able to predict axis-dependent conduction polarity in layered compounds [14] by only considering the m_{ij}^{*-1} tensor, the scattering time tensor τ_{ij} has not been explored, which also plays an important role in determining the sign of the thermopower. More specifically, while the τ_{ij} tensor has to be positive, the character of its energy derivative τ'_{ij} is not obvious. Indeed, the full picture of transport is complex, even in the single-band goniopolar metals.

As examples of the rich transport physics in these materials, the conduction polarities in NaSn$_2$As$_2$ measured by the Seebeck and Hall effect are opposite, and hydrodynamic electronic transport as well as phonon drag are observed in PdCoO$_2$ [15–17]. Further, NaSn$_2$As$_2$ was discovered to be superconducting by s-wave pairing [18–21], and an optical study of PdCoO$_2$ reveals unexpected features due to the coupling of in-plane charge carriers with cross-plane optical phonons [22]. Moreover, these goniopolar systems also show a quasi-two-dimensional crystal structure and band topology, in which hydrodynamic electron flow has been discovered recently [7,23–25]. In each of these cases, electron scattering with both electrons and phonons (especially the latter) leads to unconventional transport behavior, and significant deviation from the traditional Fermi liquid regime under certain conditions. While the cross section of the Fermi surface in the xy plane of PdCoO$_2$ is nearly hexagonal, the star-shaped Fermi surface in NaSn$_2$As$_2$ has both convex and concave segments, which, as we will show later, lead to even more complex unexpected transport behaviors. These findings naturally raise a fundamental question as to whether the original theoretical proposal is valid in assuming the relaxation time to be a scalar in goniopolar materials.

[*]yaxianwang@seas.harvard.edu
[†]prineha@seas.harvard.edu

125122-1

To elucidate the electron scattering physics of such open Fermi surface systems, in this paper we study $NaSn_2As_2$ as a "typical" goniopolar metal, and we establish from first principles the microscopic origins of electron scattering. Furthermore, we establish the anisotropic lifetime tensor τ_{ij} to investigate the axis-dependent scattering times, i.e., τ_{xx} and τ_{zz}. We present the electron-electron scattering time (τ_{ee}) and the momentum relaxing electron-phonon scattering time ($\tau_{e\text{-ph}}^{MR}$) with a dependence on both temperature and electron chemical potential, showing that the electron-phonon coupling dominates the scattering near the Fermi energy. We show how the anisotropic electron lifetimes contribute to the conduction polarity and modify the macroscopic thermopower reported in the earlier work [11] on this material by explicitly examining the energy dependence of τ'_{ij}, which confirms that both the xx and zz components are positive. To address the opposite sign of the Hall coefficients, we calculate the electron velocity evolution under a magnetic field, and we find that the real-space electron orbits self-intersect due to the concave segments of the Fermi surface [26,27]. This work sheds light on the anisotropic electron lifetimes in goniopolar materials, and it establishes a complete theoretical framework to understand goniopolar transport by providing important first-principles insights into electron scattering microscopics on open Fermi surfaces.

II. SCATTERING MECHANISMS

In a metal with a considerable electron density of states at the Fermi level, there are two primary scattering channels: electron-electron (e-e) scattering and electron-phonon (e-ph) scattering. We utilize the maximally localized Wannier functions (MLWFs) to evaluate both scattering matrices from first-principles calculations following a similar approach to that presented in earlier work [28–35], with computational details given in the SI [36–43]. The electron lifetimes for various scattering events, i.e., e-e scattering through the screened Coulomb interaction and e-ph scattering involving an electron and a phonon, are determined by the imaginary part of electron self-energy as $\tau_{ee} = \hbar/2 \, Im\Sigma_{ee}$ and $\tau_{e\text{-ph}} = \hbar/2 \, Im\Sigma_{e\text{-ph}}$, and τ_{total} can be obtained by Matthiessen's rule (see the Methods section in the SI [36]). While τ_{ee} can be obtained from the electron quasiparticle self-energy, $\tau_{e\text{-ph}}$ relies on the details of crystal momentum, i.e., on the phonon dispersion. $NaSn_2As_2$ ($R\bar{3}m$, space group No. 166) has a van der Waals (vdW) Zintl phase [Fig. 1(a)], with five atoms in a rhombohedral primitive cell [44]. There is one electron band crossing the Fermi level E_F in $NaSn_2As_2$ [Fig. 1(b)], and analysis of the partial density of states (PDOS) [Fig. 1(b)] shows that this band arises from the mixing of Sn-s, p and As-p orbitals. We therefore used 16 Wannier functions centered at the s, p_x, p_y, and p_z orbitals of each of the two Sn and As atomic sites. The band structure reproduced using the Wannier functions shows good agreement with the density functional theory (DFT) results, especially for the band that crosses E_F, which determines the transport properties for a metal. The system has 15 phonon branches. There is no ao gap, i.e., energy separation between the acoustic and optical modes, but a big energy gap of about 10 meV exists between the lower- and higher-energy

optical modes [Fig. S1(a) in the supplemental information (SI) [19,36,44]].

A brief comparison between $Im\Sigma_{ee}$ and $Im\Sigma_{e\text{-ph}}$ shows that e-e scattering is prominent along the cross-plane (Γ-Z) direction. This is because the weak interlayer van der Waals (vdW) force in quasi-two-dimensional $NaSn_2As_2$ leads to optical phonons with little dispersion along Γ-Z. However, the electron band is highly dispersive even along the stacking direction. A closer examination of this electron band along the high-symmetry path in the Brillouin zone shows that $Im\Sigma_{e\text{-ph}}$ dominates most wave vectors along the in-plane direction (Γ-L and Γ-F) [Fig. S1(c) in the SI [36]]. Given that the three acoustic phonon branches have comparable slopes along all directions, the enhanced $Im\Sigma_{e\text{-ph}}$ along the in-plane direction indicates that the optical phonon modes also contribute to scattering electrons. While a qualitative comparison can be made by inspecting the high-symmetry path, the strong anisotropy of this material and the complexity of its Fermi surface require knowledge of contributions from all the electronic states. The electron-electron and electron-phonon scattering times at wave vectors sampled across the whole Brillouin zone and at energies above and below the Fermi level are shown in Fig. 1(c). τ_{ee} peaks at E_F, and its rapid reduction away from E_F can be described by an $(\varepsilon - E_F)^2$ dependence, with $\mu = \varepsilon - E_F$ being the electron chemical potential. This resembles a Fermi liquid feature similar to that of simple metals (see Fig. S2 in the SI for comparison with Al and Cu [36]). However, there is another peak located at around $E_F + 1.6$ eV, likely due to the second lowest energy conduction band that has a high electronic density of states [Fig. 1(b), right panel]. Moreover, unlike Al and Cu, where $\tau_{e\text{-ph}}$ clearly dominates in a wide energy range, in $NaSn_2As_2$ there is an energy window at around $E_F + 1.3$ eV where τ_{ee} with certain momenta is smaller than $\tau_{e\text{-ph}}$. This is also indicated by the larger $Im\Sigma_{ee}$ along the cross-plane direction.

Prior work has shown that $NaSn_2As_2$ has a negligible magnetoresistance [11], indicating that there is only one microscopic length scale near the Fermi surface. Therefore, in the present work, we focus on studying $\tau_{e\text{-ph}}$ within ± 0.8 eV of E_F. To get the momentum-relaxing electron lifetime $\tau_{e\text{-ph}}^{MR}$ that is more relevant to the transport properties, we account for the small-angle scattering which commonly happen at low temperatures by weighing the electron scattering rate $\tau_{e\text{-ph}}^{-1}(n\mathbf{k})$ with $v_{n\mathbf{k}} \cdot v_{n\mathbf{k}}$ (see the Methods section in the SI [36]). The temperature dependence of τ_{ee}, $\tau_{e\text{-ph}}^{MR}$, together with τ_{total} obtained by Matthiessen's rule is shown in Fig. 1(d). Without altering the electron chemical potential, $\tau_{e\text{-ph}}^{MR}$ determines the electron scattering time from 5 to 300 K, especially in the medium temperature range 25–100 K. Normally, the resistivity that is governed by the interactions between electrons and acoustic phonons is expected to have a T^1 dependence at temperatures above $\sim\Theta_D/5$, where Θ_D is the Debye temperature and it has been evaluated to be ~ 198 K in $NaSn_2As_2$ from specific-heat measurement [11]. In the temperature region from 50 to 300 K, we fit the data with $\tau^{-1}(T) = A + BT^\alpha$ and obtained $\alpha \approx 1.18$, showing a substantial deviation from the T^1 dependence. This further demonstrates that the optical phonon modes also play an important role in scattering electrons in this system. At very low T ($<< \Theta_D$), the resistivity of a metal usually follows T^5, in which T^3 is from
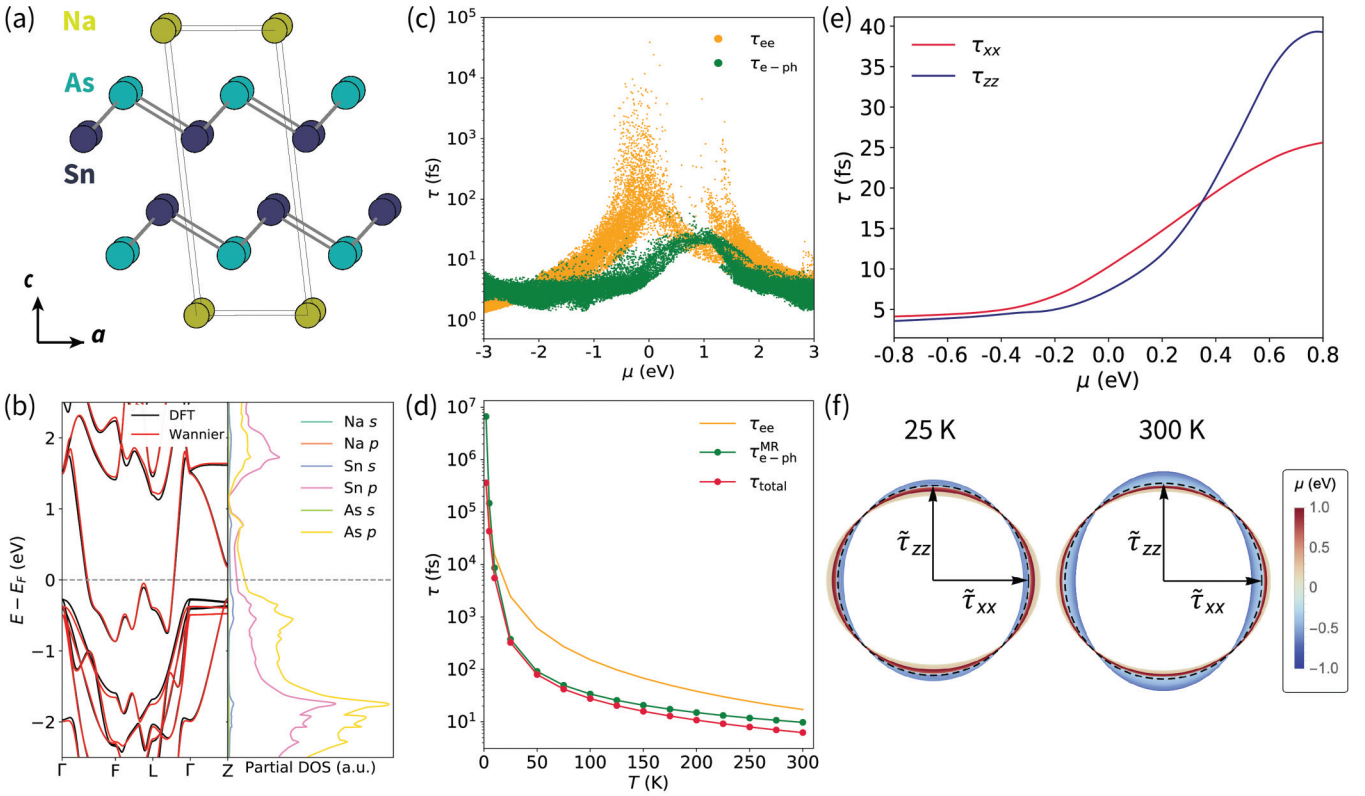
FIG. 1. (a) Lattice structure of the primitive cell of $NaSn_2As_2$ viewed from [1 0 0], highlighting the vdW layers and Na atoms as electron donors. (b) Left: Band structures obtained from both DFT (black) and maximally localized Wannier functions (red). Right: Partial density of states of $NaSn_2As_2$, indicating that the Fermi surface has mainly Sn-s, p and As-p characters. (c) Comparison of e-ph and e-e scattering times with dependence of electron chemical potential $\mu = \varepsilon - E_F$, highlighting that e-ph interaction is dominating near the E_F. The wide range of τ distribution is because electronic states at wave vectors across the Brillouin zone have different scattering rates. (d) Temperature dependence of $\tau_{\text{e-ph}}^{\text{MR}}$, τ_{ee}, and τ_{total} obtained by Matthiessen's rule. (e) Axis-dependent momentum relaxing $[\tau_{\text{e-ph}}]_{ij}$ with dependence of electron chemical potential calculated at 300 K, showing that both $\tau'_{xx} = \frac{d\tau_{xx}}{dE}$ and $\tau'_{zz} = \frac{d\tau_{zz}}{dE}$ have positive signs at E_F with their positive slopes. (f) Normalized $\tilde{\tau}_{xx}$ and $\tilde{\tau}_{zz}$ at various electron chemical potentials calculated at 25 and 300 K, showing that the scattering time anisotropy is more significant at high temperatures. The black dashed circle is the isotropic reference as a guide.

the phonon density of states and T^2 is from the small-angle scattering, where $\theta \approx \vec{q}/\vec{k} \approx T/\Theta_D$. Below 50 K (2–25 K in this context), we fit the data with similar $\tau^{-1}(T) = A' + B'T^{\alpha'}$ and obtained $\alpha' \approx 3.89$. Possible reasons that they deviate from the T^5 dependence here include the following. First, in the present work, the momentum relaxing electron-phonon scattering time $\tau_{\text{e-ph}}^{\text{MR}}$ is weighed by $1 - \cos\theta$ when integrating $\tau_{\text{e-ph}}^{-1}(n\mathbf{k})$ at a certain temperature and thus could have a less significant temperature dependence. Second, $NaSn_2As_2$ is a quasi-two-dimensional material, whose phonon density of states is expected to follow a temperature dependence between T^2 and T^3, the latter of which is typical of a three-dimensional solid.

The macroscopic transport properties are determined mostly by the states near E_F; therefore, we present the anisotropic electron-phonon lifetimes in momentum space across the Fermi surface at different temperatures in Fig. 2. The Fermi surface of $NaSn_2As_2$ has an open concave shape, which is consistent with previous work [11]. Though the Fermi surface features long lifetimes at similar regions at elevated temperatures (5 K and above), the strong contrast, i.e., the range of three orders of magnitude, of the lifetimes
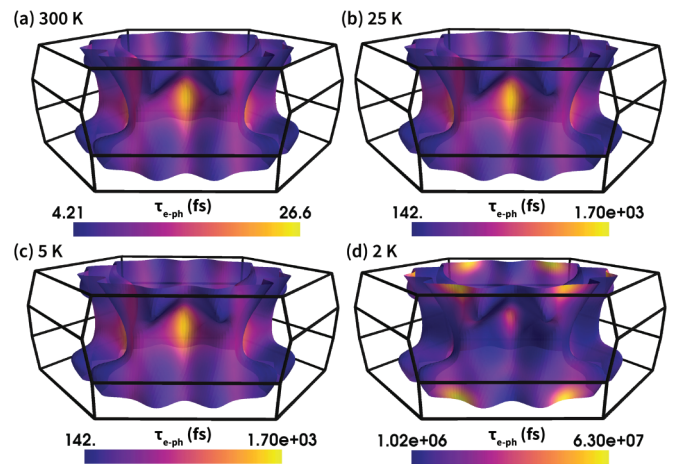

FIG. 2. Anisotropic $\tau_{\text{e-ph}}^{\text{MR}}(n\mathbf{k})$ in fs distribution on the Fermi surface, highlighting the appearance of the large lifetime regions across the Fermi surface with decreasing temperature (a) 300 K, (b) 25 K, (c) 5 K, and (d) 2 K. There is a significant disparity between the lifetimes at low temperatures near 25 K, where the value of $\tau_{\text{e-ph}}^{\text{MR}}(n\mathbf{k})$ on the Fermi surface varies over three orders of magnitude.

at a "moderate" temperature 25 K is noteworthy. Such long-lived electrons could possibly allow momentum-conserving scattering to dominate the charge flow and thus lead to hydrodynamic transport [7,23–25,33], which we hope will encourage further experimental investigation. Moreover, the distinct feature at 2 K of long lifetimes instead being located at the zone boundary rather than at the center is worth further study, as it may help us to understand the superconducting phase discovered in this vdW compound at 1.3 K for stoichiometric NaSn$_2$As$_2$ [18] and 2.1 K for Na$_{1+x}$Sn$_{2-x}$As$_2$ [20]. Further, we recall that similar systems, namely delafossites PdCoO$_2$ and PtCoO$_2$, are also single-band metals with hexagonal open Fermi surface shapes similar to that of NaSn$_2$As$_2$. Although the subtlety of the Fermi surface is affected by the crystal symmetry and orbital mixing, the similarity of their Fermi surface topology warrants that PdCoO$_2$ and PtCoO$_2$ are also goniopolar, the former of which is predicted in Ref. [12]. More specifically, the Fermi surface of NaSn$_2$As$_2$ is mostly composed of Sn- and As-p orbitals [Fig. 1(b)], while the Fermi surface of PdCoO$_2$ arises from mixing of Pd-5s, 4d_{z^2}, 4$d_{x^2-y^2}$, and 4d_{xy} orbitals [45]. However, since both NaSn$_2$As$_2$ and PdCoO$_2$ have a quasi-two-dimensional crystal structure and open, concave Fermi surface topology, we believe our results on the electron lifetimes, as well as our analysis later, could be extended to these delafossites.

III. AXIS-DEPENDENT $\tau_{e\text{-ph}}^{MR}$

The physical origin of the axis-dependent conduction polarity in NaSn$_2$As$_2$ is proposed to be the concave Fermi surface topology, which manifests as the opposite signs of its in-plane (α_{xx}) and cross-plane (α_{zz}) thermopowers, each evaluated with the ratio of $\sigma'_{ij} = \frac{d\sigma_{ij}}{dE}$ over σ_{ij} at $\varepsilon = E_F$ following

$$\alpha_{ij} = -\frac{\pi^2 k_B^2 T}{3q} \left\{ \frac{N'}{N}\bigg|_{\varepsilon=E_F} + \frac{\tau'_{ij}}{\tau_{ij}}\bigg|_{\varepsilon=E_F} + \frac{[m_{ij}^{*-1}]'}{[m_{ij}^{*-1}]}\bigg|_{\varepsilon=E_F} \right\},$$
(1)

where k_B is the Boltzmann constant, and primed quantities denote derivatives with respect to energy. Here, the carrier density N is a scalar, but the inverse effective mass m_{ij}^{*-1} and τ_{ij} are tensors. As pointed out earlier, the analytical model proposed in Ref. [11] has only considered the effect from m_{ij}^{*-1}, but not τ_{ij}, which we will provide in this work. After establishing that electron-phonon scattering dominates the electron lifetimes in NaSn$_2$As$_2$, we now examine the axis-dependent $[\tau_{e\text{-ph}}]_{ij}$ and discuss its contribution to the overall thermopower. We obtain the anisotropic $[\tau_{e\text{-ph}}]_{ij}$ by weighing each momentum relaxing lifetime at different states $\tau_{e\text{-ph}}^{MR}(n\mathbf{k})$ by $v_{n\mathbf{k}} \otimes v_{n\mathbf{k}}$ (see the Methods section in the SI [36]). The axis-resolved τ_{xx} and τ_{zz} with a dependence on the electron chemical potential at 300 K are shown in Fig. 1(e). As mentioned earlier, we restrict the energy window to within 0.8 eV with respect to E_F, where we can safely assume that $\tau_{e\text{-ph}}^{MR}$ determines the electron lifetimes. Both τ_{xx} and τ_{zz} have a positive slope near E_F, with an anisotropy ratio $\tau_{zz}/\tau_{xx} < 2$. Examination of τ'_{xx}/τ_{xx} and τ'_{zz}/τ_{zz} confirms they both have positive sign near the Fermi level ($|\varepsilon - E_F| <$
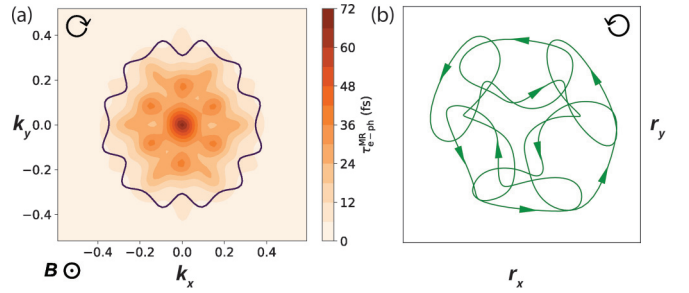

FIG. 3. (a) Fermi surface cross section at the $k_z = 0.25c^*$ plane, where c^* is the cross-plane reciprocal-lattice vector, outlined by a solid line in purple, with the color map showing the room-temperature momentum relaxing lifetime distribution. (b) Electron orbits in real space for the Fermi surface shape in (a), highlighting the self-intersection due to the presence of concave areas on the Fermi surface loop.

0.2 eV). Figure 1(f) shows the comparison of principal components of $[\tau_{e\text{-ph}}]_{ij}$ normalized as $\tilde{\tau}_{zz,xx} = \sqrt{\tau_{zz,xx}/(\sqrt{\tau_{zz}}\sqrt{\tau_{xx}})}$ at different temperatures. The change of the scattering time anisotropy versus electron chemical potential is much smaller at lower temperature, which suggests that the axis-dependent conduction polarity in NaSn$_2$As$_2$ does indeed originate from its Fermi surface topology instead of the electron scattering. However, the anisotropic lifetimes do contribute a substantial portion to the overall thermopower. According to previous work [11], only considering the band topology, the predicted α_{xx} is -2 μV/K at 300 K, which was measured to be -2 and -6 μV/K in two different samples. On the other hand, α_{zz} was predicted to be $+21$ μV/K while measured to be $+8$ and $+10$ μV/K [11]. According to Eq. (1), the lifetime tensor will contribute $-\frac{\pi^2 k_B^2 T}{3e} \times \frac{\tau'_{xx}}{\tau_{xx}}$ to α_{xx} and $-\frac{\pi^2 k_B^2 T}{3e} \times \frac{\tau'_{zz}}{\tau_{zz}}$ to α_{zz}, both of which are negative. Therefore including the contribution from the anisotropic scattering time tensor decreases the absolute value of α_{zz} but increases the absolute value of α_{xx}, thus bringing the theoretical results in considerably better agreement with the experimental measurements. Overall, the study of axis-dependent lifetimes allows us to build a complete theory for goniopolar transport. It further suggests that a calculation of electron lifetimes is indeed an important step in determining whether or not a material is goniopolar, even if an analysis of the electronic band curvatures may give a reasonable estimation for promising candidates.

IV. HALL CONDUCTIVITY

While we conclude that the goniopolar thermoelectric response in NaSn$_2$As$_2$ originates from the anisotropic effective-mass tensor instead of the scattering time tensor, another question left unanswered is why the conduction polarity is flipped in the Hall-effect measurement. Specifically, with negative α_{xx} indicating electron conduction along the in-plane direction, the Hall coefficient is measured to be positive, indicating positive charge carriers, i.e., holes. To solve this puzzle, we explicitly calculate the electron velocity evolution under an applied magnetic field.

Figure 3(a) shows the Fermi surface as a loop on a slice of the xy plane at the midpoint of Γ-Z, i.e., $k_z = 0.25c^*$, where c^* is the cross-plane reciprocal-lattice vector. Since we are moving away from the zone center, the Fermi surface shows much more complexity than a simple hexagonal shape. There are multiple concave and convex regions along k_x and k_y. With color showing the distribution of room-temperature $\tau_{\text{e-ph}}^{\text{MR}}$ on such a slice, the long lifetime spots on the Fermi surface loop can be seen, which are the six concave segments with smaller curvature, as visualized by the color highlighting the same position in Fig. 2. Applying a magnetic field along k_z will impose a Lorentz force on the electron velocities, the evolution of which can be evaluated assuming a constant relaxation time (see the Methods section in the SI [26,36,46]), and it is shown in Fig. 3(b). The electron orbit in real space is clearly complicated and is subject to the subtlety of the Fermi surface. The most pronounced feature is that it self-intersects multiple times where the Fermi surface contains concave segments. With arrows guiding the eye, one can see that the circulation of electrons has opposite directions. According to Ong [27], the Hall conductivity is determined by the circulation area of the "Fermi surface" in the mean free path space. Due to the lattice symmetry, we treat the in-plane electron scattering time as isotropic [47]. Thus the evolution of $\mathbf{v}(\mathbf{k})$ can be directly mapped into the mean free path space since $\mathbf{r}(\mathbf{k}) = \mathbf{v}(\mathbf{k})\tau$. Here, the outer and inner loops show opposite circulation, i.e., clockwise in the momentum space but anticlockwise in the mean free path space, resulting in the sign flipping of the Hall conductivity.

V. CONCLUSIONS AND OUTLOOK

In summary, we present a first-principles investigation of anisotropic electron scattering on an open Fermi surface. We study a single-band metal $NaSn_2As_2$, which was shown to have opposite conduction polarity along in-plane and cross-plane directions originating from its band topology, to reveal how the electron lifetimes affect its macroscopic transport properties. We evaluate the electron lifetimes due to scattering with both electrons and phonons with energy and momentum resolution, and we find that the electron-phonon scattering dominates the electron lifetimes within 0.8 eV of the Fermi level, in a temperature range of 5–300 K. We further study the axis-dependent momentum relaxing lifetime τ_{xx} and τ_{zz} at different electron chemical potentials, and we discuss their contribution to the macroscopic thermopower and the overall axis-dependent conduction polarity. Finally, we address the opposite conduction polarity observed in the Hall effect by calculating the real-space electron orbits in the presence of an external magnetic field, and we show how the self-intersection leads to opposite circulation, which flips the sign of the Hall coefficients.

Our work closes the gap left between electron scattering and goniopolar thermoelectric behavior, and it consolidates the theoretical frameworks, which will facilitate more targeted material searches in the future. Interestingly, our analysis of $NaSn_2As_2$, as well as its similarity with $PdCoO_2$, suggests the strong possibility of hydrodynamics in this and similar goniopolar materials, which we expect will spark experimental investigation. These together can serve as a foundation for understanding the electron scattering rates in materials with axis-dependent conduction polarity, as well as drawing attention to broader research interests regarding exotic transport behaviors in systems with nontrivial Fermi surface topology, such as topological semimetals.

[1] M. Cutler and N. F. Mott, Phys. Rev. **181**, 1336 (1969).

[2] J. Jan, Helv. Phys. Acta **41**, 957 (1968).

[3] N. Kumar, Y. Sun, M. Nicklas, S. J. Watzman, O. Young, I. Leermakers, J. Hornung, J. Klotz, J. Gooth, K. Manna, V. Süß, S. N. Guin, T. Förster, M. Schmidt, L. Muechler, B. Yan, P. Werner, W. Schnelle, U. Zeitler, J. Wosnitza, S. S. P. Parkin, C. Felser, and C. Shekhar, Nat. Commun. **10**, 2475 (2019).

[4] F. Arnold, C. Shekhar, S.-C. Wu, Y. Sun, R. D. dos Reis, N. Kumar, M. Naumann, M. O. Ajeesh, M. Schmidt, A. G. Grushin, J. H. Bardarson, M. Baenitz, D. Sokolov, H. Borrmann, M. Nicklas, C. Felser, E. Hassinger, and B. Yan, Nat. Commun. **7**, 11615 (2016).

[5] P. He, C.-H. Hsu, S. Shi, K. Cai, J. Wang, Q. Wang, G. Eda, H. Lin, V. M. Pereira, and H. Yang, Nat. Commun. **10**, 1290 (2019).

[6] M. Besser, R. D. dos Reis, F.-R. Fan, M. O. Ajeesh, Y. Sun, M. Schmidt, C. Felser, and M. Nicklas, Phys. Rev. Mater. **3**, 044201 (2019).

[7] C. Q. Cook and A. Lucas, Phys. Rev. B **99**, 235148 (2019).

[8] M. N. Ali, L. M. Schoop, C. Garg, J. M. Lippmann, E. Lara, B. Lotsch, and S. S. P. Parkin, Sci. Adv. **2**, e1601742 (2016).

[9] O. Pavlosiuk, M. Kleinert, P. Swatek, D. Kaczorowski, and P. Wiśniewski, Sci. Rep. **7**, 12822 (2017).

[10] R. Singha, A. Pariari, G. K. Gupta, T. Das, and P. Mandal, Phys. Rev. B **97**, 155120 (2018).

[11] B. He, Y. Wang, M. Q. Arguilla, N. D. Cultrara, M. R. Scudder, J. E. Goldberger, W. Windl, and J. P. Heremans, Nat. Mater. **18**, 568 (2019).

[12] K. P. Ong, D. J. Singh, and P. Wu, Phys. Rev. Lett. **104**, 176601 (2010).

[13] V. Eyert, R. Frésard, and A. Maignan, Chem. Mater. **20**, 2370 (2008).

[14] Y. Wang, K. G. Koster, A. M. Ochs, M. R. Scudder, J. P. Heremans, W. Windl, and J. E. Goldberger, J. Am. Chem. Soc. **142**, 2812 (2020).

[15] N. Nandi, T. Scaffidi, P. Kushwaha, S. Khim, M. E. Barber, V. Sunko, F. Mazzola, P. D. C. King, H. Rosner, P. J. W. Moll, M. König, J. E. Moore, S. Hartnoll, and A. P. Mackenzie, npj Quantum Mater. **3**, 66 (2018).

[16] P. J. W. Moll, P. Kushwaha, N. Nandi, B. Schmidt, and A. P. Mackenzie, Science **351**, 1061 (2016).

[17] M. D. Bachmann, A. L. Sharpe, A. W. Barnard, C. Putzke, M. König, S. Khim, D. Goldhaber-Gordon, A. P. Mackenzie, and P. J. W. Moll, Nat. Commun. **10**, 5081 (2019).

[18] Y. Goto, A. Yamada, T. D. Matsuda, Y. Aoki, and Y. Mizuguchi, J. Phys. Soc. Jpn. **86**, 123701 (2017).

[19] K. Ishihara, T. Takenaka, Y. Miao, O. Tanaka, Y. Mizukami, H. Usui, K. Kuroki, M. Konczykowski, Y. Goto, Y. Mizuguchi, and T. Shibauchi, Phys. Rev. B **98**, 020503(R) (2018).

[20] H. Yuwen, Y. Goto, R. Jha, A. Miura, C. Moriyoshi, Y. Kuroiwa, T. D. Matsuda, Y. Aoki, and Y. Mizuguchi, Jpn. J. Appl. Phys. **58**, 083001 (2019).

[21] E. J. Cheng, J. M. Ni, F. Q. Meng, T. P. Ying, B. L. Pan, Y. Y. Huang, D. C. Peets, Q. H. Zhang, and S. Y. Li, Europhys. Lett. **123**, 47004 (2018).

[22] C. C. Homes, S. Khim, and A. P. Mackenzie, Phys. Rev. B **99**, 195127 (2019).

[23] J. A. Sulpizio, L. Ella, A. Rozen, J. Birkbeck, D. J. Perello, D. Dutta, M. Ben-Shalom, T. Taniguchi, K. Watanabe, T. Holder, R. Queiroz, A. Principi, A. Stern, T. Scaffidi, A. K. Geim, and S. Ilani, Nature (London) **576**, 75 (2019).

[24] L. Ella, A. Rozen, J. Birkbeck, M. Ben-Shalom, D. Perello, J. Zultak, T. Taniguchi, K. Watanabe, A. K. Geim, S. Ilani, and J. A. Sulpizio, Nat. Nanotechnol. **14**, 480 (2019).

[25] T. Holder, R. Queiroz, T. Scaffidi, N. Silberstein, A. Rozen, J. A. Sulpizio, L. Ella, S. Ilani, and A. Stern, Phys. Rev. B **100**, 245305 (2019).

[26] S. Zhang, Q. Wu, Y. Liu, and O. V. Yazyev, Phys. Rev. B **99** 035142 (2019).

[27] N. P. Ong, Phys. Rev. B **43**, 193 (1991).

[28] M.-N. Su, C. J. Ciccarino, S. Kumar, P. D. Dongare, S. A. H. Jebeli, D. Renard, Y. Zhang, B. Ostovar, W.-S. Chang, P. Nordlander, N. J. Halas, R. Sundararaman, P. Narang, and S. Link, Nano Lett. **19**, 3091 (2019).

[29] P. Narang, L. Zhao, S. Claybrook, and R. Sundararaman, Adv. Opt. Mater. **5**, 1600914 (2017).

[30] A. M. Brown, R. Sundararaman, P. Narang, W. A. Goddard, and H. A. Atwater, ACS Nano **10**, 957 (2015).

[31] C. A. C. Garcia, J. Coulter, and P. Narang, Phys. Rev. Res. **2**, 013073 (2020).

[32] J. Coulter, G. B. Osterhoudt, C. A. C. Garcia, Y. Wang, V. M. Plisson, B. Shen, N. Ni, K. S. Burch, and P. Narang, Phys. Rev. B **100**, 220301 (2019).

[33] J. Coulter, R. Sundararaman, and P. Narang, Phys. Rev. B **98**, 115130 (2018).

[34] C. J. Ciccarino, T. Christensen, R. Sundararaman, and P. Narang, Nano Lett. **18**, 5709 (2018).

[35] P. Narang, R. Sundararaman, A. S. Jermyn, W. A. Goddard, and H. A. Atwater, J. Phys. Chem. C **120**, 21056 (2016).

[36] See Supplemental Material at http://link.aps.org/supplemental/10.1103/PhysRevB.102.125122 for more details on materials properties, methods, and computational details.

[37] R. Sundararaman, K. Letchworth-Weaver, K. A. Schwarz, D. Gunceler, Y. Ozhabes, and T. Arias, SoftwareX **6**, 278 (2017).

[38] K. F. Garrity, J. W. Bennett, K. M. Rabe, and D. Vanderbilt, Comput. Mater. Sci. **81**, 446 (2014).

[39] S. Grimme, J. Comput. Chem. **27**, 1787 (2006).

[40] F. Giustino, M. L. Cohen, and S. G. Louie, Phys. Rev. B **76**, 165108 (2007).

[41] S. Poncé, E. Margine, C. Verdi, and F. Giustino, Comput. Phys. Commun. **209**, 116 (2016).

[42] P. Giannozzi, S. Baroni, N. Bonini, M. Calandra, R. Car, C. Cavazzoni, D. Ceresoli, G. L. Chiarotti, M. Cococcioni, I. Dabo et al., J. Phys.: Condens. Matter **21**, 395502 (2009).

[43] A. D. Corso, Comput. Mater. Sci. **95**, 337 (2014).

[44] M. Q. Arguilla, J. Katoch, K. Krymowski, N. D. Cultrara, J. Xu, X. Xi, A. Hanks, S. Jiang, R. D. Ross, R. J. Koch, S. Ulstrup, A. Bostwick, C. Jozwiak, D. W. McComb, E. Rotenberg, J. Shan, W. Windl, R. K. Kawakami, and J. E. Goldberger, ACS Nano **10**, 9500 (2016).

[45] K. P. Ong, J. Zhang, J. S. Tse, and P. Wu, Phys. Rev. B **81**, 115120 (2010).

[46] Q. Wu, S. Zhang, H.-F. Song, M. Troyer, and A. A. Soluyanov, Comput. Phys. Commun. **224**, 405 (2018).

[47] G. Varnavides, A. S. Jermyn, P. Anikeeva, C. Felser, and P. Narang, arXiv:2002.08976.